Research in Astron. Astrophys. Vol.0 (20xx) No.0, 000–000
http://www.raa-journal.org *http://www.iop.org/journals/raa*

***R**esearch in*
***A**stronomy and*
***A**strophysics*

arXiv:1411.4349v1 [astro-ph.GA] 17 Nov 2014

CO observations of a sample towards nearby galaxies

Fa-Cheng Li[1,2], Yuan-Wei Wu[1] and Ye Xu[1]

[1] Purple Mountain Observatory, & Key Laboratory for Radio Astronomy, Chinese Academy of Sciences, Nanjing 210008, China; *lifc@pmo.ac.cn*
[2] University of Chinese Academy of Sciences, Beijing 100039, China

Abstract We have simultaneously observed ^{12}CO, ^{13}CO, and C^{18}O (J=1−0) rotational transitions in the centers of a sample of 58 nearby spiral galaxies using the 13.7-m millimeter-wave telescope of the Purple Mountain Observatory. Forty-two galaxies were detected in ^{13}CO emission, but there was a null detection for C^{18}O emission with a sigma upper limit of 2 mK. Central beam ratios, $\mathcal{R}$, of ^{12}CO and ^{13}CO range mostly from 5 to 13, with an average value of 8.1±4.2, which is slightly lower than previous estimates for normal galaxies. Clear correlations are found between ^{12}CO and ^{13}CO luminosities. An average X-factor of $1.44 \pm 0.84 \times 10^{20}$ cm^{-2} (K km s^{-1})$^{-1}$ is slightly lower than that in the Milky Way.

Key words: galaxies:ISM–molecules:galaxies–millimeter lines:ISM–star formation:ISM

1 INTRODUCTION

Molecular hydrogen, H_2, constitutes a dominant part of molecular clouds in the interstellar medium (ISM) in galaxies and is most closely related to star formation. The current method of studying molecular clouds in external galaxies involves the observation of rotational transitions of carbon dioxide, CO. H_2 lacks a dipole moment and therefore, quadrupole or vibrational transitions cannot be excited under typical cold temperature conditions in giant molecular clouds (GMCs). Rotational transitions of CO can easily be generated by collisions with H_2, particularly the line from the first excited level to ground, J=1−0, can be excited under the condition of very low temperatures and density of only 10 K and 300 cm^{-3} respectively. Thus, ^{12}CO, as well as its isotopic variants, remain the most straightforward and reliable tracer of H_2 in molecular clouds. In addition, there is a well-known CO−H_2 conversion factor, called the X factor, and it is defined as

$$X_{\rm CO} = \frac{N({\rm H_2})}{I_{\rm CO}}\ [{\rm cm^{-2}\ (K\ km\ s^{-1})^{-1}}], \quad (1)$$

where $N({\rm H_2})$ is the column density of H_2 in cm^{-2} and $I_{\rm CO}$ is the integrated line intensity of ^{12}CO.

The first CO detections in external galaxies were carried out by Rickard et al. (1975) and Solomon & de Zafra (1975). Later, Young et al. (1995) published the Five Colleges Radio Astronomy Observatory (FCRAO) extragalactic CO survey at $\lambda = 2.6$ mm of a large sample of 300 galaxies with 1412 positions using the 14 m telescope at 45″ resolution. The detection rate is 79% and 193 galaxies were observed in multiple positions. Braine et al. (1993) observed both ^{12}CO(1−0) and ^{12}CO(2−1) emission from the centers of 81 nearby spiral galaxies using the 30-m telescope at the Institut de Radioastronomie Millimetrque (IRAM) at a resolution of 23″ and 12″ for ^{12}CO(1−0) and ^{12}CO(2−1), respectively, and finding an average (and median) ^{12}CO(2−1) to ^{12}CO(1−0) line ratio to be 0.89±0.06.

Solomon et al. (1997) also used the IRAM 30-m telescope to observe ^{12}CO(1−0) transitions in 37 ultraluminous infrared galaxies and discovered that interacting galaxies also have relatively high CO luminosity. There are plenty of other CO surveys of nearby galaxies using either single-dishes or even interferometer telescopes that have aimed to map the molecular gas distribution or kinematics within galaxies and have worked out properties of molecular gas clouds from galaxy to galaxy (Sakamoto et al. 1999; Nishiyama et al. 2001; Helfer et al. 2003; Leroy et al. 2009). However, most of these surveys are based on ^{12}CO J=1−0, J=2−1 or even higher rotational transitions, while there are few systematic studies of CO isotopologue transitions of a larger sample of galaxies has yet to be published. This is probably because ^{12}CO J=1−0 is found to not be an accurate measure of the amount of molecular gas, however, ^{13}CO emission with lower opacity may give more reliable constraints on the H_2 column density.

Sage & Isbell (1991) presented observations of ^{13}CO (1−0) emission from 16 nearby spiral galaxies using the 12-m telescope at the National Radio Astronomy Observatory. They found the ratio of ^{12}CO (1−0) and ^{13}CO (1−0) emittance to be insensitive to variations in global parameters such as inclination angle and Hubble type. The detection revealed a range of central beam ratios from 5 to 16.6, mostly from 7 to 11. Aalto et al. (1995) studied molecular gas in 32 infrared-bright galaxies, which consists mostly of starbursts. They presented several line ratios, among which they suggested that the ratio of ^{12}CO/^{13}CO (1−0) can be a measurement of the cloud environment in galaxies. Paglione et al. (2001) performed a mapping survey of ^{12}CO and ^{13}CO J=1−0 emissions along the major axes of 17 nearby galaxies. Their work resulted in an average central ^{12}CO/^{13}CO intensity ratio of 11.6±1.9 implying that the X-factor is probably lower in most galactic nuclei. A non-liner correlation between CO and far-infrared luminosity exists in galaxies because luminous galaxies have a higher star formation efficiency (SFE) (Solomon & Sage 1988; Young & Scoville 1991; Gao & Solomon 2004). Taniguchi & Ohyama (1998) collected previous observational results of ^{12}CO and ^{13}CO emissions and compared far-infrared luminosity with that of ^{12}CO and ^{13}CO, respectively. They found that the ^{13}CO depression in luminous starburst mergers may account for a higher abundance ratio of ^{12}CO and ^{13}CO than that in normal galaxies. Solomon & Vanden Bout (2005) and Daddi et al. (2010) further confirmed the validity of this correlation when studying high-redshift star forming galaxies.

In order to systemically study the physical properties of external galaxies, we present simultaneous observations of ^{12}CO, ^{13}CO, and C^{18}O J=1−0 emissions from the centers of 58 nearby galaxies, mostly spiral, using the Purple Mountain Observatory (PMO) 13.7-m millimeter radio telescope. And it is the second time we carry out observations towards nearby galaxies using this telescope after Tan et al. (2011). The observations and sample selection are described in Section 2. We then present results with detected CO spectra and derived parameters in Section 3. The analysis and discussions are in Section 4 and finally the summary is in Section 5.

2 SAMPLE AND OBSERVATIONS

2.1 Sample selection

We selected a sample of 58 nearby galaxies from the FCRAO Extragalactic CO Survey (Young et al. 1995). The selection criteria were as follows: (1) $I(^{12}\mathrm{CO}) \geq 3$ K km s^{-1}, where K is in antenna temperature. Strong ^{12}CO emission usually indicates a relatively high detection rate of isotopic variants. (2) 10h≤R.A≤13h and Decl.≥-10°, in order to not conflict with the galactic time in the northern sky. Physical properties of the Infrared Astronomical Satellite (IRAS) data are summarized in Table 1, which are obtained from the IRAS Revised Bright Galaxy Sample (RGBS) (Sanders et al. 2003) and the SIMBAD database.

Table 1 Basic Properties of the Sample

Galaxy					IR size		
Name	Type	R.A. DECL. (J2000)	cz (km s^{-1})	D (Mpc)	major×minor (arcmin)		$T_{\rm dust}$ (K)
(1)	(2)	(3)	(4)	(5)	(6)	(7)	(8)
M 066	Sb	11:20:15.026 +12:59:28.64	740	10.04	6.64×3.65		34.71
M 108	Sc	11:11:30.967 +55:40:26.84	698	13.85	7.91×1.74		33.07
NGC3079	S	10:01:57.924 +55:40:48.00	1142	18.19	4.49×1.08		34.67
NGC3169	Sb	10:14:15.099 +03:27:58.03	1305	20.61	2.73×2.02		31.24
NGC3184	Sc	10:18:16.985 +41:25:27.77	593	12.58	6.72×5.72		29.71
NGC3593	S0	11:14:37.002 +12:49:04.87	578	5.04	3.48×1.43		35.25
NGC3628	Sbc	11:20:17.018 +13:35:22.16	825	10.04	10.58×2.54		35.54
NGC3631	Sc	11:21:02.944 +53:10:09.95	1158	21.58	4.19×4.02		31.07
NGC3672	Sc	11:25:02.476 −09:47:43.44	1899	27.70	2.97×1.13		31.30
NGC3675	Sb	11:26:08.584 +43:35:09.30	804	12.69	4.45×2.00		29.15
NGC3690	Sm	11:28:31.600 +58:33:44.00	3159	47.74	1.61×1.41		47.31
NGC3810	Sc	11:40:58.737 +11:28:16.07	1001	15.36	3.05×2.08		32.12
NGC3893	Sc	11:48:38.207 +48:42:38.84	892	16.35	2.88×2.13		33.06
NGC3938	Sc	11:52:49.453 +44:07:14.63	800	14.75	4.00×3.80		30.57
NGC4030	Scdr	12:00:23.643 −01:05:59.87	1427	24.50	2.67×2.35		31.41
NGC4038	Sc	12:01:52.480 −18:52:02.90	1563	21.54	5.20×3.10		35.55
NGC4039	Sc	12:01:53.700 −18:53:08.00	1563	21.54	3.10×1.60		35.55
NGC4041	Sc	12:02:12.173 +62:08:14.23	1243	22.78	1.70×1.39		33.67
NGC4051	SBab	12:03:09.686 +44:31:52.54	728	13.11	4.73×2.60		33.04
NGC4088	Sc	12:05:34.189 +50:32:20.50	696	13.37	4.39×2.11		33.35
NGC4096	Sc	12:06:01.161 +47:28:42.09	523	9.63	5.76×1.73		30.21
NGC4102	Sb	12:06:23.115 +52:42:39.42	859	16.89	1.78×0.98		39.20
NGC4157	Sb	12:11:04.365 +50:29:04.85	790	13.30	4.94×0.89		31.02
NGC4194	I	12:14:09.573 +54:31:36.03	2555	40.33	0.67×0.46		45.18
NGC4212	Sc	12:15:39.375 +13:54:05.30	-81	15.29	2.97×1.42		32.15
NGC4254	Sc	12:18:49.625 +14:24:59.36	2403	15.29	4.50×4.27		32.65
NGC4258	Sbc	12:18:57.620 +47:18:13.39	448	7.10	11.14×5.46		-
NGC4273	SBc	12:19:56.063 +05:20:36.12	2400	15.29	1.71×1.20		33.27
NGC4293	Sap	12:21:12.891 +18:22:56.64	893	16.50	5.29×1.80		-
NGC4298	Sc	12:21:32.790 +14:36:21.78	1141	15.29	2.97×1.78		28.71
NGC4302	Sc	12:21:42.477 +14:35:51.94	1149	19.20	5.37×0.64		-
NGC4303	SABbc	12:21:54.950 +04:28:24.92	1570	15.29	4.64×3.48		34.39
NGC4312	Sa	12:22:31.359 +15:32:16.51	153	16.50	3.39×0.88		30.75
NGC4321	Sc	12:22:54.899 +15:49:20.57	1571	15.20	7.23×5.64		31.89
NGC4402	Sb	12:26:07.566 +13:06:46.06	237	15.29	2.97×0.59		30.04
NGC4414	Sc	12:26:27.089 +31:13:24.76	720	17.68	2.86×1.60		32.92
NGC4419	SBa	12:26:56.433 +15:02:50.72	-261	15.29	2.54×0.81		34.26
NGC4433	Sbc	12:27:38.610 −08:16:42.42	2913	41.68	1.52×0.55		36.60
NGC4457	SB0/Sa	12:28:59.011 +03:34:14.19	882	12.40	2.00×1.36		34.84
NGC4490	Sd	12:30:36.710 +41:38:26.60	641	10.48	5.32×2.29		35.83
NGC4501	Sbc	12:31:59.216 +14:25:13.48	2284	15.29	5.47×2.41		29.94
NGC4527	Sb	12:34:08.496 +02:39:13.72	1771	15.29	4.62×1.57		34.51
NGC4535	SBc	12:34:20.310 +08:11:51.94	1957	15.77	5.84×2.92		31.09
NGC4536	Sc	12:34:27.129 +02:11:16.37	1802	14.92	4.61×2.40		39.51
NGC4567	Sc	12:36:32.703 +11:15:28.33	2262	15.29	3.72×2.19		31.50
NGC4568	Sc	12:36:34.292 +11:14:19.07	2262	15.29	4.06×1.59		31.50

Table 1 – *Continued*

Galaxy					IR size		
Name	Type	R.A. DECL. (J2000)	cz (km s^{-1})	D (Mpc)	major×minor (arcmin)		$T_{\rm dust}$ (K)
(1)	(2)	(3)	(4)	(5)	(6)	(7)	(8)
NGC4569	Sab	12:36:49.816 +13:09:46.33	-235	15.29	6.92×2.77		31.57
NGC4579	Sab	12:37:43.527 +11:49:05.46	1519	7.73	4.60×3.22		28.86
NGC4631	Sc	12:42:08.009 +32:32:29.44	630	15.29	9.25×2.78		35.93
NGC4647	Sc	12:43:32.542 +11:34:56.89	1415	15.29	2.58×2.04		30.97
NGC4654	SBcd	12:43:56.638 +13:07:34.86	1037	12.82	4.47×2.01		31.16
NGC4666	Sbc	12:45:08.676 −00:27:42.88	1495	20.65	3.32×0.93		33.29
NGC4691	S0a	12:48:13.600 −03:19:57.70	1124	21.71	2.80×2.30		38.37
NGC4710	S0a	12:49:38.958 +15:09:55.76	1125	15.29	3.73×0.90		33.67
NGC4736	Sb	12:50:53.148 +41:07:12.55	323	4.83	4.13×3.27		37.40
NGC4818	Sab	12:56:48.907 −08:31:31.08	1051	9.37	3.34×1.60		41.33
NGC4826	Sb	12:56:43.696 +21:40:57.57	349	3.09	6.82×3.89		33.76
NGC4845	Sb	12:58:01.242 +01:34:32.09	1224	15.09	3.85×1.08		32.93

Notes: Column (1): Names of the sample galaxies. Column (2): Morphological types taken from the SIMBAD database (http://simbad.u-strasbg.fr/simbad/). Column (3): Adopted tracking center of observed galaxies; Units of right ascension are hours, minutes, and seconds, and units of declination are degrees, arcminutes, and arcseconds. The data in Column (4)-(5) except for NGC4258, NGC4293, NGC4302, NGC4312 and NGC4457 are taken from Sanders et al. (2003). Column (4): The heliocentric radial velocity computed as c times the redshift z. Column (5): Distances including luminosity ones and metric ones. Column (6)-(7): Infrared angular sizes taken from mostly 2MASS data using SIMBAD. Column (8): Dust temperature derived from the RBGS IRAS 60 μm/100 μm color assuming an emissivity that is proportional to the frequency ν; those without RBGS(Sanders et al. 2003) data are calculated following Sanders & Mirabel (1996) using *IRAS Point Source Catalog* (PSC:1988).

2.2 Observations

We made observations between February and June 2011 and supplementary observations between September and October 2011 and also December 2012, using the PMO 13.7-m millimeter-wave telescope located at Delingha, Qinghai, China. The observations were made after the newly developed 3×3 multi-beam sideband separation superconducting spectroscopic array receiver (SSAR) was added. The receiver employs a two-sideband superconductor-insulator-superconductor (SIS) mixer, which allowed us to simultaneously observe ^{12}CO J=1−0 emission in the upper sideband (USB) and ^{13}CO and C^{18}O J=1−0 emissions in the lower sideband (LSB). A high definition Fast Fourier Transition Spectrometer (FFTS) as backend enabled a bandwidth of 1 GHz and a velocity resolution of 0.16 km s^{-1}at 115.271 GHz. Single-point observations using beam 5 of SSAR were done in the "ON-OFF" position switching mode, with a pointing accuracy of nearly 5″. The Half Power Beam Width was 52″ at 115.271 GHz and the main beam efficiency, $\eta_{\rm mb}$, for USB and LSB were 0.46 and 0.5 respectively between February and June 2011 and were 0.44 and 0.48 during October 2011[1]. Typical system temperatures were 220 K at 115.271 GHz and 130 K at 110.201 GHz during our observations.

3 RESULTS

3.1 Data reduction

We reduced the data using CLASS, which is a part of the GILDAS [2] software package. The original data included individual scans. Of each spectrum, line-free channels that exhibited positive or negative

[1] See the Status Report http://www.radioast.csdb.cn/zhuangtaibaogao.php

[2] http://www.iram.fr/IRAMFR/GILDAS/

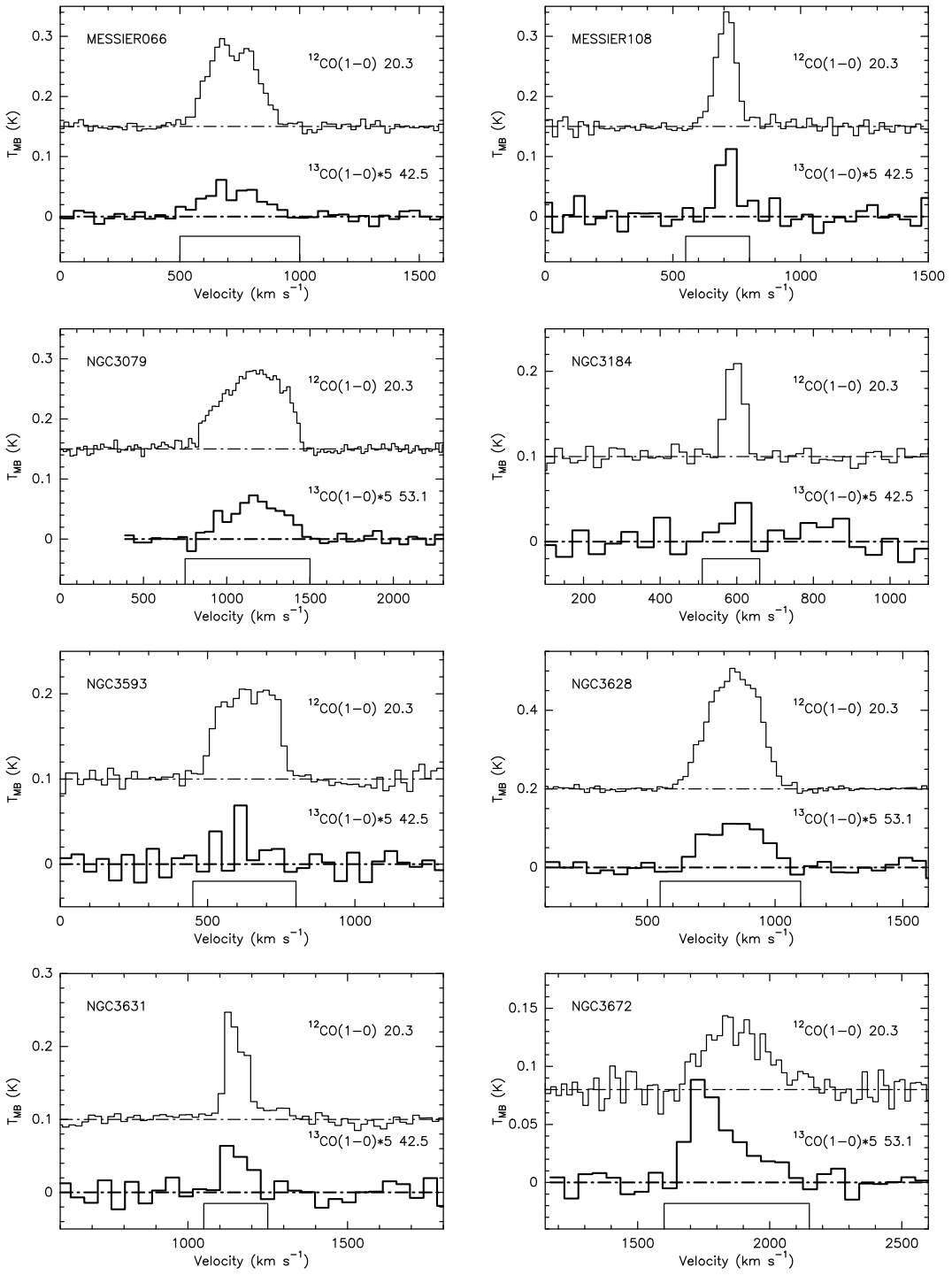

Fig. 1 Observed spectra of ^{12}CO (thin lines) and ^{13}CO (thick lines) in the central regions of ^{13}CO detected galaxies. Velocities are the radio velocities with respect to LSR. The spectra of ^{13}CO emissions are multiplied by 5 for comparison. The spectra are on the scale of main beam temperature. All the spectra were smoothed to a velocity resolution of about 20 km s^{-1}for ^{12}CO and about 40 km s^{-1}for ^{13}CO in order to limit the rms noise. The number right after the spectrum label is specified velocity resolution for individual source. The window for emission feature is drawn on the bottom of the axis box in each plot.

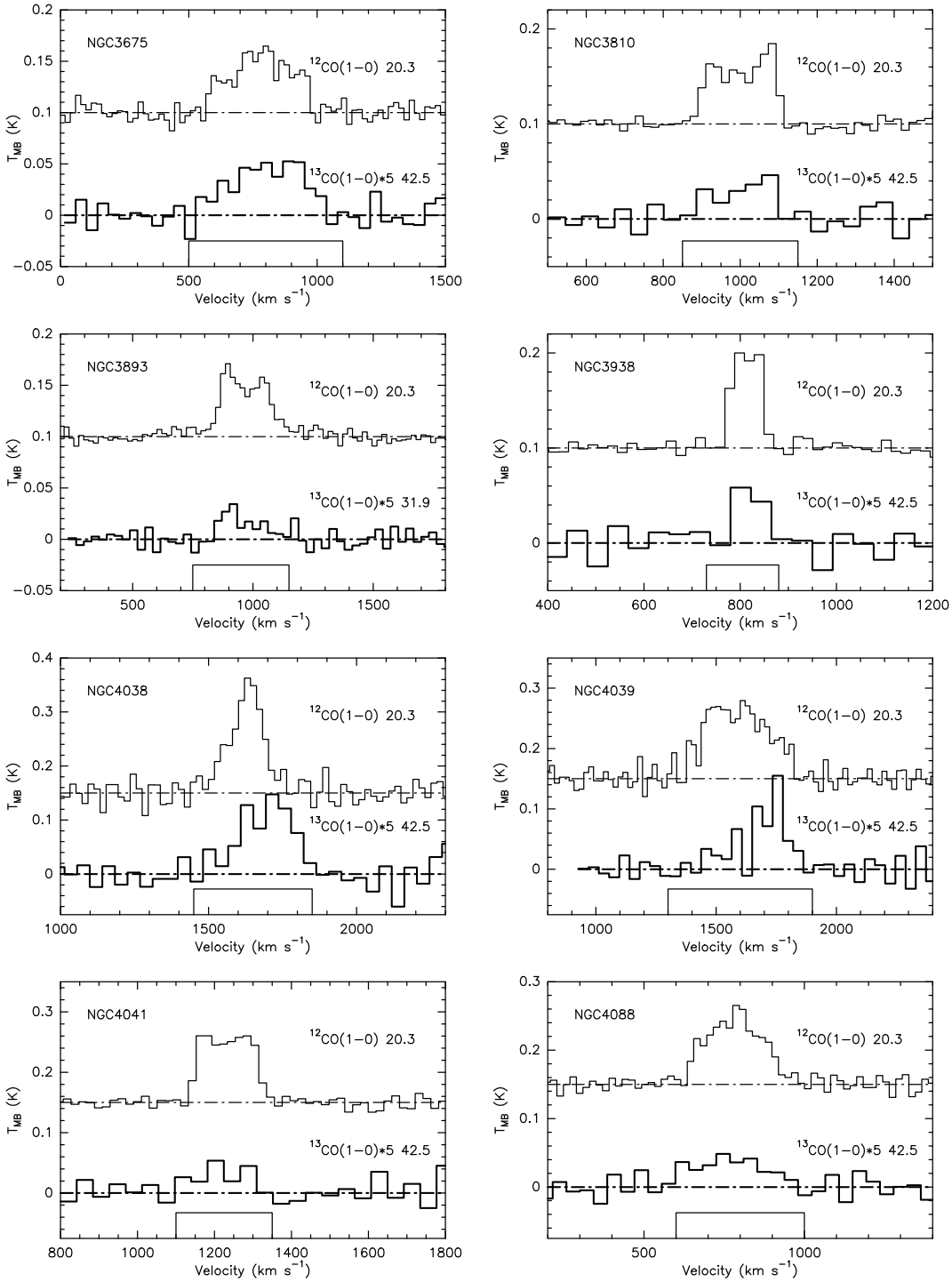

Fig. 1 – *Continued*

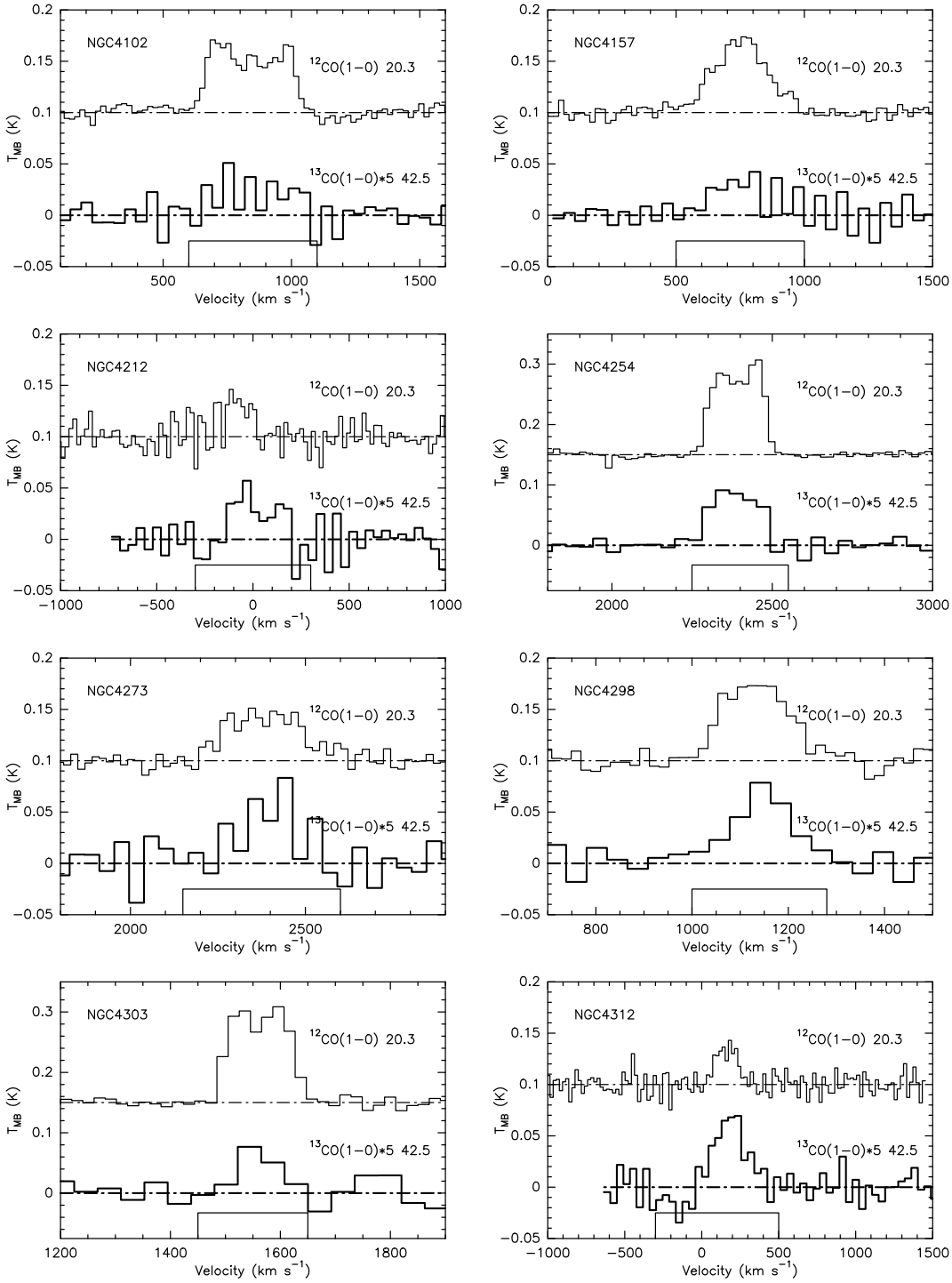

Fig. 1 *– Continued*

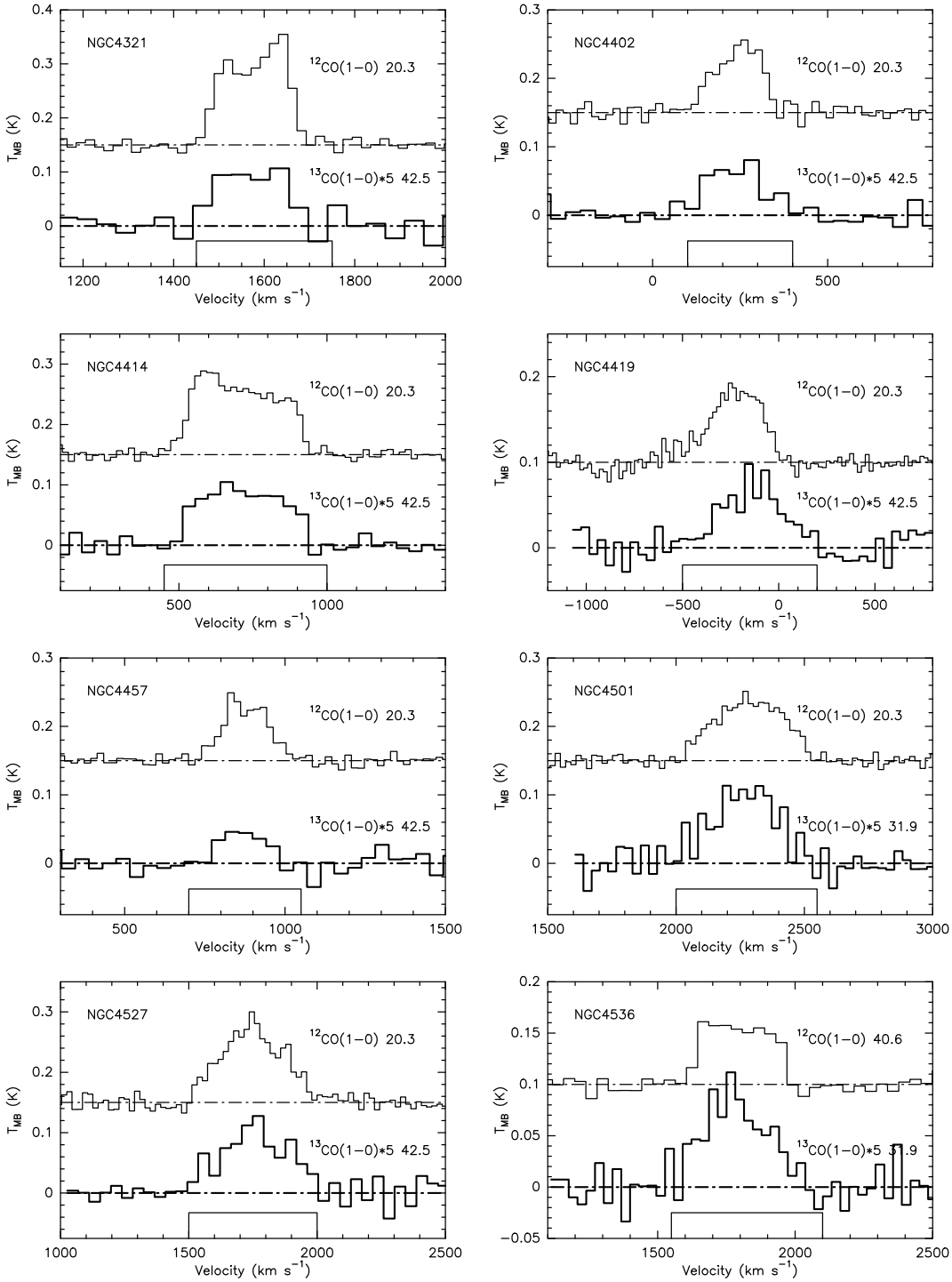

Fig. 1 *– Continued*

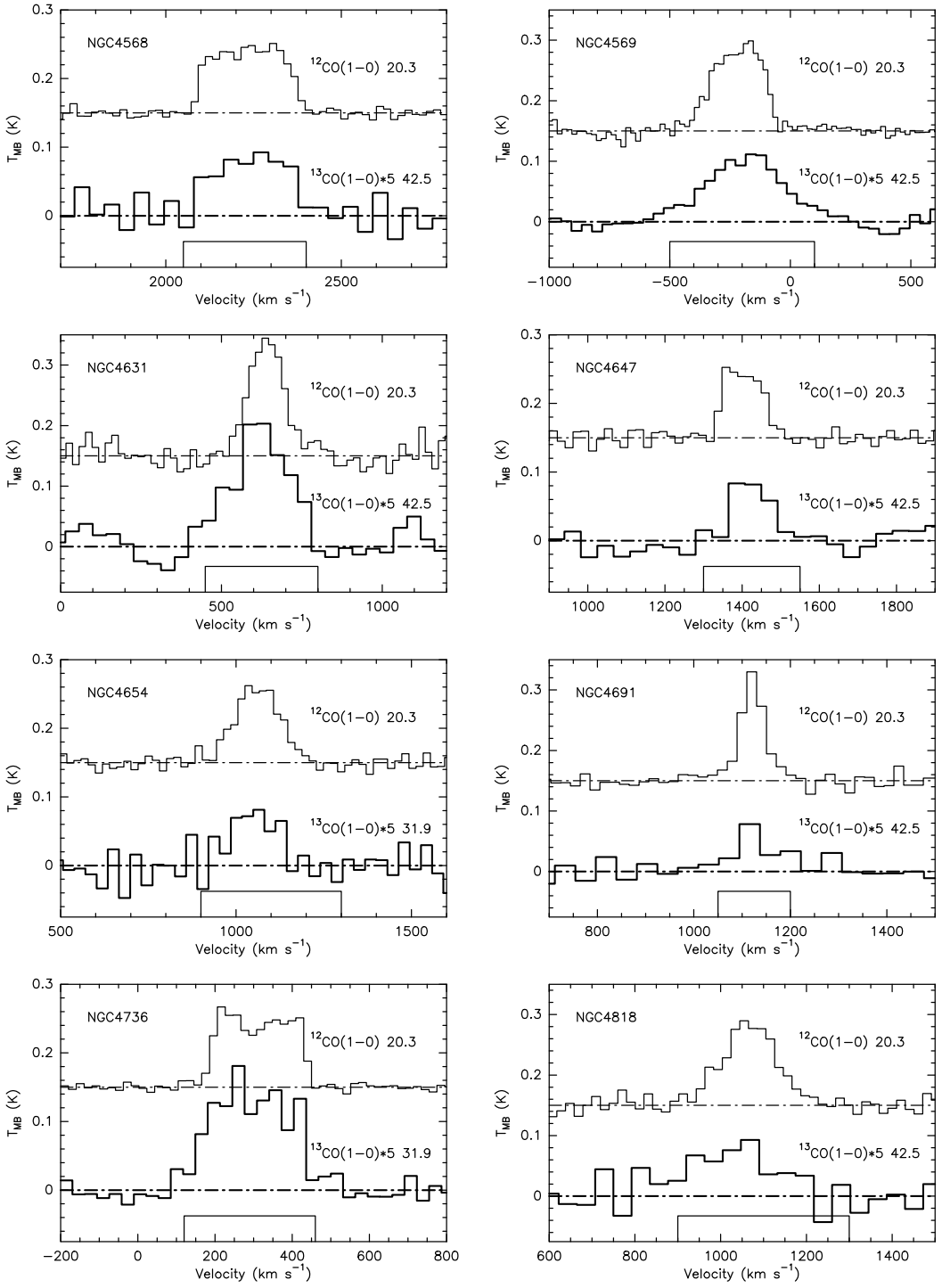

Fig. 1 – *Continued*

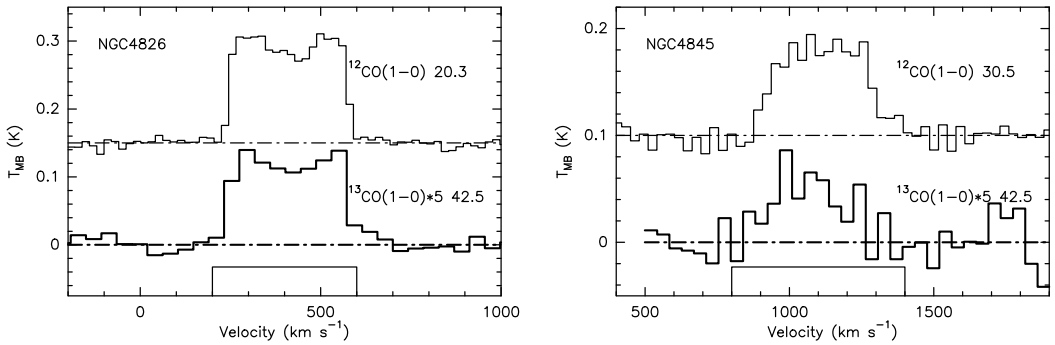

Fig. 1 *– Continued*

spikes more than 5σ above the rms noise were blanked or substituted with values interpolated from adjacent ones. This was only done after properly setting the velocity range limits for each spectrum and a liner baseline was subtracted from it. We then examined every spectrum and then we chose those with a relatively bad baseline and an abnormally high rms noise. Due to unstable spectrum baselines and bad weather conditions, a considerable part of the data was discarded. After converting the temperature scale to $T_{\rm mb}$ from $T_{\rm A}^*$ of the spectra and dividing by $\eta_{\rm mb}$, we then averaged the converted data weighting by the inverse square of the rms noise, sigma. Note however that data from different observational seasons were treated differently. The final averaged spectra of each source were smoothed to a velocity resolution of about 20 km s^{-1}for ^{12}CO and about 40 km s^{-1}for ^{13}CO in order to limit the rms noise. Each averaged spectrum was fitted using the GAUSS method and the results are presented in the next subsection.

3.2 Observational results

We observed simultaneously ^{12}CO, ^{13}CO, and C^{18}O emissions at the centers of 58 nearby galaxies, among which 42 were detected in ^{13}CO emission with a signal-to-noise ratio of more than 3, while C^{18}O emission was too weak to be detected in any galaxy with an upper limit of 2 mK (1 σ). Both ^{12}CO and ^{13}CO line profiles agree very well with similar centroid velocities and line widths in most cases, as shown in Fig. 1. All of the spectra were smoothed to a velocity resolution of about 20 km s^{-1}for ^{12}CO and about 40 km s^{-1}for ^{13}CO to improve the signal-to-noise ratio, which are given in Table 2. We do not show those ^{12}CO spectra without ^{13}CO detection since one can easily find them in the literature.

The integrated intensity, $I_{\rm CO}$, can be obtained by integrating $T_{\rm mb}$ over the line emission feature,

$$I_{\rm CO} \equiv \int T_{\rm mb} dv \ [\rm K\ km\ s^{-1}], \tag{2}$$

And the error of the integrated intensity is estimated through the following formula (Elfhag et al. 1996),

$$\delta I = \sigma_{\rm rms} \sqrt{\frac{\Delta v dV}{(1-\Delta v/W)}}\ [\rm K\ km\ s^{-1}], \tag{3}$$

where $T_{\rm rms}$ is the rms noise temperature, Δv is the line width of the emission feature, dV is the spectrum velocity resolution, and W is the entire velocity range of each spectrum. These properties for each spectrum is presented in Fig. 1: W is taken from the visible velocity range in each plot; Δv is the window for emission feature drawn on the bottom; dV is labeled. For those without the detection of

^{13}CO, $2\delta I_{13}$ upper limits were given based on estimates by using the expected line width from the detected ^{12}CO lines at exactly the same position. The peak velocities and line widths come from a Gaussian fit. The ratio of ^{12}CO and ^{13}CO integrated intensity is defined as

$$\mathcal{R} \equiv \frac{\int T_{\rm mb}(^{12}{\rm CO})dv}{\int T_{\rm mb}(^{13}{\rm CO})dv}. \quad (4)$$

Table 2 Observational Results

	^{12}CO(1−0)				^{13}CO(1−0)				
Galaxy	$I \pm \delta I$ (K km s^{-1})	$\sigma_{\rm rms}$ (mK)	V (km s^{-1})	ΔV	$I \pm \delta I$ (K km s^{-1})	$\sigma_{\rm rms}$ (mK)	V (km s^{-1})	ΔV	$\mathcal{R}$
(1)	(2)	(3)	(4)	(5)	(6)	(7)	(8)	(9)	(10)
M 066	33.89±0.67	5.54	719	233	2.75±0.22	1.28	714	283	12.32±1.02
M 108	17.94±0.67	8.58	708	89	2.01±0.37	3.29	713	73	8.93±1.68
NGC3079	59.17±0.96	6.38	1160	425	5.11±0.28	1.17	1176	378	11.58±0.66
NGC3169	31.66±1.33	7.69	1182	447	<1.50	2.46	–	–	>21.11
NGC3184	6.52±0.44	7.42	594	52	0.56±0.25	2.89	601	42	11.64±5.26
NGC3593	24.34±0.78	7.86	637	212	1.02±0.34	2.37	616	42	23.86±7.99
NGC3628	72.66±0.59	4.44	840	226	5.92±0.59	2.73	843	252	12.27±1.23
NGC3631	11.29±0.51	7.33	1147	76	1.17±0.27	2.66	1146	91	9.65±2.27
NGC3672	15.58±1.31	9.76	1870	265	3.55±0.33	1.53	1769	186	4.39±0.55
NGC3675	17.13±1.05	7.37	786	282	3.26±0.42	2.04	814	312	5.25±0.75
NGC3690	24.29±0.66	4.87	3093	260	<0.46	1.36	–	–	>52.80
NGC3810	12.42±0.47	5.07	1006	183	1.39±0.27	2.03	1016	181	8.94±1.77
NGC3893	13.63±0.53	5.08	963	238	0.83±0.20	1.51	927	153	16.42±4.01
NGC3938	7.47±0.33	5.42	813	66	0.85±0.23	2.56	820	42	8.79±2.41
NGC4030	21.95±1.74	14.29	1454	290	<2.24	6.35	–	–	>9.80
NGC4038	28.62±2.00	18.49	1632	127	5.74±0.76	4.83	1701	189	4.99±0.75
NGC4039	39.93±1.96	14.06	1584	313	4.47±0.69	3.40	1734	146	8.93±1.45
NGC4041	18.33±0.65	7.86	1234	152	1.39±0.46	3.84	1218	146	13.19±4.39
NGC4051	10.66±0.53	4.71	705	141	<1.02	3.65	–	–	>10.45
NGC4088	21.90±1.07	9.73	782	208	2.32±0.46	2.89	758	263	9.44±1.93
NGC4096	6.58±0.72	6.40	546	136	<0.60	1.83	–	–	>10.97
NGC4102	21.03±0.68	5.51	825	335	1.63±0.39	2.16	834	310	12.90±3.12
NGC4157	17.88±0.61	4.94	751	241	1.93±0.44	2.44	764	300	9.26±2.14
NGC4194	4.02±1.02	7.98	2515	139	<1.36	3.66	–	–	>2.96
NGC4212	5.27±1.55	11.72	-85	156	1.45±0.59	3.09	-13	218	3.63±1.82
NGC4254	25.55±0.49	5.44	2393	168	3.20±0.24	1.82	2380	164	7.98±0.62
NGC4258	52.70±1.27	8.80	423	348	<2.46	6.80	–	–	>21.42
NGC4273	11.77±0.81	6.52	2385	245	2.36±0.59	3.29	2405	178	4.99±1.29
NGC4293	12.18±0.70	8.47	929	171	<0.54	2.24	–	–	>22.56
NGC4298	12.69±0.72	7.74	1132	157	2.17±0.30	2.22	1148	137	5.85±0.87
NGC4302	13.25±1.67	18.48	1134	190	<1.28	4.87	–	–	>10.35
NGC4303	19.28±0.49	6.44	1563	118	1.31±0.41	3.72	1557	73	14.72±4.62
NGC4312	5.93±1.46	9.46	162	160	2.57±0.58	2.58	184	224	2.31±0.77
NGC4321	30.07±0.78	8.07	1585	162	3.60±0.56	3.98	1572	168	8.35±1.32
NGC4402	15.82±0.85	9.24	247	153	2.79±0.37	2.82	235	194	5.67±0.81
NGC4414	44.11±0.90	6.45	692	336	6.55±0.40	2.01	708	315	6.73±0.43
NGC4419	26.82±1.41	9.50	-219	308	5.78±0.66	3.07	-135	333	4.64±0.58
NGC4433	20.60±1.01	7.40	2946	273	<1.08	2.74	–	–	>19.07

Table 2 – *Continued*

Galaxy	^{12}CO(1−0)				^{13}CO(1−0)				$\mathcal{R}$
	$I \pm \delta I$ (K km s^{-1})	$\sigma_{\rm rms}$ (mK)	V (km s^{-1})	ΔV	$I \pm \delta I$ (K km s^{-1})	$\sigma_{\rm rms}$ (mK)	V (km s^{-1})	ΔV	
(1)	(2)	(3)	(4)	(5)	(6)	(7)	(8)	(9)	(10)
NGC4457	14.51±0.62	6.23	875	164	1.52±0.41	2.81	864	148	9.55±2.61
NGC4490	3.18±0.43	6.02	609	125	<0.72	3.47	–	–	>4.42
NGC4501	29.66±0.91	6.86	2288	315	6.58±0.59	3.56	2268	294	4.51±0.43
NGC4527	37.20±1.21	9.80	1749	286	6.90±0.61	3.44	1759	311	5.39±0.51
NGC4535	21.87±1.23	10.60	1993	199	<2.28	6.76	–	–	>9.59
NGC4536	17.33±1.13	5.88	1786	274	4.81±0.56	3.32	1776	271	3.60±0.48
NGC4567	12.33±0.47	5.58	2273	167	<0.58	2.39	–	–	>12.92
NGC4568	24.46±0.61	5.97	2236	230	4.33±0.68	4.61	2247	238	5.65±0.90
NGC4569	36.23±1.20	8.61	-214	234	7.92±0.48	2.39	-186	346	4.57±0.32
NGC4579	11.38±1.08	9.81	1492	272	<1.30	4.09	–	–	>8.71
NGC4631	11.73±0.74	9.00	639	125	2.18±0.41	3.45	622	199	5.38±1.07
NGC4647	26.42±1.87	18.63	1401	111	8.36±0.72	4.96	1422	108	3.16±0.35
NGC4654	16.81±0.97	8.54	1061	147	2.12±0.68	4.81	1051	146	7.93±2.58
NGC4666	35.61±1.16	8.58	1525	268	<3.16	8.06	–	–	>11.26
NGC4691	10.82±0.58	9.51	1122	56	1.08±0.31	3.50	1122	97	10.02±2.93
NGC4710	14.97±1.03	7.43	1086	290	<1.06	2.61	–	–	>14.12
NGC4736	24.31±0.43	4.16	308	224	7.38±0.38	2.95	293	240	3.29±0.18
NGC4818	21.54±1.41	11.63	1067	146	3.21±0.91	5.21	1021	232	6.71±1.95
NGC4826	48.17±0.65	5.88	409	298	8.40±0.33	2.08	413	306	5.73±0.24
NGC4845	30.70±1.52	8.69	1118	320	3.55±0.77	3.74	1054	274	8.65±1.92

Notes: Column (1):Names of the sample galaxies. Column (2):^{12}CO integrated intensities and uncertainties, calculated from eq. (2) and eq. (3). Column (3):Baseline noises of spectra in mK. Column (4)&(5):Gaussian fitting results of peak velocities and FWHM line widths. Column (6)−(9):Results for ^{13}CO, for non-detections, 2-sigma upper limits are given. Column (10): The ratios of ^{12}CO and ^{13}CO integrated intensities and their uncertainties.

3.3 Derived properties

The derived physical parameters, such as the H_2 column density, the CO luminosity, and the gas mass, are presented in Table 3. We assumed that the CO and its isotopic variants are approximately under the conditions of local thermodynamic equilibrium (LTE) when activating transitions and CO transitions are optically thick. Therefore we estimated the average optical depth of ^{13}CO from (Sage & Isbell 1991)

$$\tau^{13} \simeq -\ln\left[1 - \frac{\int T_{\rm R}^{*}(^{13}{\rm CO})dv}{\int T_{\rm R}^{*}(^{12}{\rm CO})dv}\right], \quad (5)$$

where $T_{\rm R}^{*}$ should be corrected for a filling factor and therefore this is only an averaged estimation over all of the unresolved clouds in the beam.

Due to the beam dilution effect of remote molecular clouds in remote galaxies, we could hardly measure the excitation temperature, $T_{\rm ex}$, directly. We present the cold dust color temperature, $T_{\rm dust}$, calculated from IRAS far infrared data assuming a dust emissivity, $\propto \nu^1$, in Table 1. However, the gas and dust in the central regions of the galaxies may not couple, and therefore, we took the half value of $T_{\rm dust}$ as the gas kinetic temperature as well as the excitation temperature, $T_{\rm ex} = T_{\rm k}$.

The H_2 column density of galaxies was estimated from an empirical equation (Nishiyama et al. 2001) in the Milky Way,

$$N({\rm H_2}) = 2 \times 10^{20} \int T_{\rm mb}(^{12}{\rm CO})dv \ [{\rm cm^{-2}}], \quad (6)$$

where the coefficient is the standard galactic ^{12}CO to H_2 conversion factor, X.

Using the LTE assumption, the total column density of ^{13}CO (1-0) transition is described as (Wilson et al. 2009)

$$N(^{13}\mathrm{CO}) = 3.0 \times 10^{14} \frac{T_{\rm ex} \int \tau_{13} dv}{1 - \exp[-5.3/T_{\rm ex}]} \ [\mathrm{cm}^{-2}]. \quad (7)$$

Here, we assumed the filling factor as 1 and ^{13}CO optically thin so that there would be $T_{\rm ex}\ \tau = T_{\rm mb}$ and $T_{\rm ex} \int \tau_{13} dv = T_{\rm mb}\tau_{13}/(1 - \mathrm{e}^{-\tau_{13}})$. We then took a relatively high ratio of $N(\mathrm{H_2})/N(^{13}\mathrm{CO}) \sim 7.5 \times 10^5$ determined by the relationship between $N(^{13}\mathrm{CO})$ and visual extinction as well as $N(\mathrm{H_2})$ and $A_{\rm V}$. Consequently, we also obtained the H_2 column density from the following equation,

$$N(\mathrm{H_2})' = 7.5 \times N(^{13}\mathrm{CO}) = 2.25 \times 10^{20} \frac{\tau_{13}}{1 - \mathrm{e}^{-\tau_{13}}} \frac{\int T_{\rm mb}(^{13}\mathrm{CO}) dv}{1 - \exp[-5.3/T_{\rm ex}]} \ [\mathrm{cm}^{-2}]. \quad (8)$$

By equating the H_2 column density derived both from ^{12}CO and ^{13}CO, we can estimate the kinetic temperature as well as excitation temperature of the molecular gas in each galaxy.

The CO luminosity in K km s^{-1} pc^2 can be defined as (Taniguchi & Ohyama 1998)

$$L_{\rm CO} \equiv area \times I(\mathrm{CO}) = \frac{\pi \theta_{\rm mb}^2 D^2}{4 \ln 2} \int T_{\rm mb} dv \ [\mathrm{K\ km\ s^{-1}\ pc^2}], \quad (9)$$

where $\pi\theta_{\rm mb}^2 D^2/4\ln 2$ is the total area of a Gaussian beam source in units of pc^2 and $\theta_{\rm mb}$ is the size of the beam in arc second. Furthermore, the CO luminosity can be equivalently expressed for a source of any size in terms of the total line flux (Solomon et al. 1997),

$$L_{\rm CO} = \frac{c^2}{2k} S(\mathrm{CO}) \nu_{\rm obs}^{-2} D^2 (1+z)^{-3} = 3.25 \times 10^7 S(\mathrm{CO}) \nu_{\rm obs}^{-2} D^2 (1+z)^{-3}, \quad (10)$$

here $L_{\rm CO}$ is in K km s^{-1} pc^2, k is the Boltzmann constant, $\nu_{\rm obs}$ is the observational frequency we received, and

$$S(\mathrm{CO}) = \frac{2k\Omega \int T_{\rm mb} dv}{\lambda^2}, \quad (11)$$

is the flux of CO in Jy, where Ω is the solid angle of the source beam.

Taking the H_2 column density derived from the ^{13}CO emission, we can calibrate the X factor.

Table 3 Derived Parameters of ^{13}CO Detected Galaxies

Galaxy	τ_{13}	$N(\mathrm{H_2})$ (10^{21} cm^{-2})	$N(\mathrm{H_2})'$	log$L_{^{12}\mathrm{CO}}$ (K km s^{-1} pc^2)	log$L_{^{13}\mathrm{CO}}$	$T_{\rm ex}$ (K)	X
(1)	(2)	(3)	(4)	(5)	(6)	(7)	(8)
M 066	0.08	6.78 (0.13)	2.46(0.20)	$8.39^{+0.01}_{-0.01}$	$7.35^{+0.03}_{-0.04}$	52.88	0.72(0.06)
M 108	0.12	3.59 (0.13)	1.75(0.32)	$8.39^{+0.02}_{-0.02}$	$7.49^{+0.07}_{-0.09}$	36.86	0.98(0.18)
NGC3079	0.09	11.83 (0.19)	4.57(0.25)	$9.15^{+0.01}_{-0.01}$	$8.13^{+0.02}_{-0.02}$	49.37	0.77(0.04)
NGC3184	0.09	1.30 (0.09)	0.44(0.20)	$7.87^{+0.03}_{-0.03}$	$6.85^{+0.16}_{-0.26}$	49.67	0.67(0.30)
NGC3593	0.04	4.87 (0.16)	0.90(0.30)	$7.65^{+0.01}_{-0.01}$	$6.32^{+0.12}_{-0.18}$	107.17	0.37(0.12)
NGC3628	0.08	14.53 (0.12)	5.40(0.54)	$8.72^{+0.00}_{-0.00}$	$7.68^{+0.04}_{-0.05}$	52.64	0.74(0.07)
NGC3631	0.11	2.26 (0.10)	0.96(0.22)	$8.58^{+0.02}_{-0.02}$	$7.64^{+0.09}_{-0.11}$	40.28	0.85(0.20)
NGC3672	0.26	3.12 (0.26)	3.16(0.29)	$8.93^{+0.04}_{-0.04}$	$8.34^{+0.04}_{-0.04}$	15.39	2.03(0.25)
NGC3675	0.21	3.43 (0.21)	2.67(0.34)	$8.30^{+0.03}_{-0.03}$	$7.63^{+0.05}_{-0.06}$	19.51	1.56(0.22)
NGC3810	0.12	2.48 (0.09)	1.18(0.23)	$8.32^{+0.02}_{-0.02}$	$7.42^{+0.08}_{-0.09}$	36.91	0.95(0.19)
NGC3893	0.06	2.73 (0.11)	0.70(0.17)	$8.42^{+0.02}_{-0.02}$	$7.25^{+0.09}_{-0.12}$	72.17	0.52(0.13)

Table 3 – *Continued*

Galaxy	τ_{13}	$N(\mathrm{H_2})$	$N(\mathrm{H_2})'$	$\log L_{^{12}\mathrm{CO}}$	$\log L_{^{13}\mathrm{CO}}$	$T_{\rm ex}$	X
		$(10^{21}\ \mathrm{cm^{-2}})$		$(\mathrm{K\ km\ s^{-1}\ pc^2})$		(K)	
(1)	(2)	(3)	(4)	(5)	(6)	(7)	(8)
NGC3938	0.12	1.49 (0.07)	0.69(0.19)	$8.07^{+0.02}_{-0.02}$	$7.17^{+0.10}_{-0.14}$	36.22	0.93(0.25)
NGC4038	0.22	5.72 (0.40)	5.60(0.74)	$8.98^{+0.03}_{-0.03}$	$8.33^{+0.05}_{-0.06}$	18.23	1.96(0.29)
NGC4039	0.12	7.99 (0.39)	4.14(0.64)	$9.13^{+0.02}_{-0.02}$	$8.22^{+0.06}_{-0.07}$	36.90	1.04(0.17)
NGC4041	0.08	3.67 (0.13)	1.21(0.40)	$8.84^{+0.02}_{-0.02}$	$7.76^{+0.12}_{-0.17}$	56.94	0.66(0.22)
NGC4088	0.11	4.38 (0.21)	2.03(0.40)	$8.45^{+0.02}_{-0.02}$	$7.52^{+0.08}_{-0.10}$	39.29	0.93(0.19)
NGC4102	0.08	4.21 (0.14)	1.61(0.39)	$8.64^{+0.01}_{-0.01}$	$7.57^{+0.09}_{-0.12}$	55.60	0.77(0.19)
NGC4157	0.11	3.58 (0.12)	1.59(0.36)	$8.36^{+0.01}_{-0.02}$	$7.44^{+0.09}_{-0.11}$	38.46	0.89(0.20)
NGC4212	0.32	1.05 (0.31)	1.36(0.55)	$7.95^{+0.11}_{-0.15}$	$7.44^{+0.15}_{-0.23}$	11.77	2.58(1.30)
NGC4254	0.13	5.11 (0.10)	2.78(0.21)	$8.63^{+0.01}_{-0.01}$	$7.78^{+0.03}_{-0.03}$	32.42	1.09(0.08)
NGC4273	0.22	2.35 (0.16)	2.18(0.54)	$8.30^{+0.03}_{-0.03}$	$7.65^{+0.10}_{-0.12}$	18.24	1.85(0.48)
NGC4298	0.19	2.54 (0.14)	1.74(0.24)	$8.33^{+0.02}_{-0.03}$	$7.61^{+0.06}_{-0.06}$	22.32	1.37(0.20)
NGC4303	0.07	3.86 (0.10)	1.15(0.36)	$8.51^{+0.01}_{-0.01}$	$7.39^{+0.12}_{-0.16}$	64.15	0.60(0.19)
NGC4312	0.57	1.19 (0.29)	2.60(0.59)	$8.07^{+0.10}_{-0.12}$	$7.75^{+0.09}_{-0.11}$	5.19	4.39(1.47)
NGC4321	0.13	6.01 (0.16)	3.06(0.48)	$8.70^{+0.01}_{-0.01}$	$7.83^{+0.06}_{-0.07}$	34.16	1.02(0.16)
NGC4402	0.19	3.16 (0.17)	2.33(0.31)	$8.43^{+0.02}_{-0.02}$	$7.72^{+0.05}_{-0.06}$	21.48	1.47(0.21)
NGC4414	0.16	8.82 (0.18)	5.80(0.35)	$9.00^{+0.01}_{-0.01}$	$8.22^{+0.03}_{-0.03}$	26.52	1.32(0.08)
NGC4419	0.24	5.36 (0.28)	5.51(0.63)	$8.65^{+0.02}_{-0.02}$	$8.04^{+0.05}_{-0.05}$	16.59	2.06(0.26)
NGC4457	0.11	2.90 (0.12)	1.38(0.37)	$8.21^{+0.02}_{-0.02}$	$7.27^{+0.10}_{-0.14}$	39.79	0.95(0.26)
NGC4501	0.25	5.93 (0.18)	5.62(0.50)	$8.70^{+0.01}_{-0.01}$	$8.09^{+0.04}_{-0.04}$	15.96	1.90(0.18)
NGC4527	0.21	7.44 (0.24)	6.50(0.57)	$8.80^{+0.01}_{-0.01}$	$8.11^{+0.04}_{-0.04}$	20.16	1.75(0.16)
NGC4536	0.33	3.47 (0.23)	5.40(0.63)	$8.44^{+0.03}_{-0.03}$	$7.94^{+0.05}_{-0.05}$	11.62	3.11(0.42)
NGC4568	0.19	4.89 (0.12)	3.76(0.59)	$8.61^{+0.01}_{-0.01}$	$7.91^{+0.06}_{-0.07}$	21.38	1.54(0.24)
NGC4569	0.25	7.25 (0.24)	7.06(0.43)	$8.79^{+0.01}_{-0.01}$	$8.17^{+0.03}_{-0.03}$	16.27	1.95(0.13)
NGC4631	0.21	2.35 (0.15)	2.13(0.40)	$7.70^{+0.03}_{-0.03}$	$7.02^{+0.07}_{-0.09}$	20.11	1.81(0.36)
NGC4647	0.38	5.28 (0.37)	7.81(0.67)	$8.65^{+0.03}_{-0.03}$	$8.20^{+0.04}_{-0.04}$	9.47	2.96(0.33)
NGC4654	0.13	3.36 (0.19)	1.77(0.57)	$8.45^{+0.02}_{-0.03}$	$7.60^{+0.12}_{-0.17}$	32.16	1.05(0.34)
NGC4691	0.11	2.16 (0.12)	1.06(0.30)	$8.52^{+0.02}_{-0.02}$	$7.57^{+0.11}_{-0.15}$	42.02	0.98(0.29)
NGC4736	0.36	4.86 (0.09)	8.03(0.41)	$7.61^{+0.01}_{-0.01}$	$7.14^{+0.02}_{-0.02}$	10.12	3.30(0.18)
NGC4818	0.16	4.31 (0.28)	3.46(0.98)	$8.13^{+0.03}_{-0.03}$	$7.36^{+0.11}_{-0.14}$	26.41	1.61(0.47)
NGC4826	0.19	9.63 (0.13)	7.72(0.30)	$7.52^{+0.01}_{-0.01}$	$6.81^{+0.02}_{-0.02}$	21.79	1.60(0.07)
NGC4845	0.12	6.14 (0.30)	3.09(0.67)	$8.70^{+0.02}_{-0.02}$	$7.81^{+0.09}_{-0.11}$	35.55	1.01(0.22)

Notes: Column (1): Galaxy names of those ^{13}CO detected. Column (2): The optical depth of ^{13}CO emission derived from eq. (5). Column (3)-(4): The H_2 column density derived from ^{12}CO and ^{13}CO, respectively, from eq. (6) and eq. (8). Column (5)-(6): ^{12}CO and ^{13}CO luminosities derived from eq. (9) or eq. (10) respectively. Column (7): Excitation temperature calculated by equating the H_2 column density derived both from ^{12}CO and ^{13}CO. Column (8): The X factor, calculated by dividing H_2 column density and CO integrated intensity, in unit of $10^{20}\mathrm{cm^{-2}[K\ km\ s^{-1}]^{-1}}$.

4 DISCUSSIONS

We confirmed the detection of ^{13}CO emissions in 42 galaxies. However, this does not mean that other galaxies do not have ^{13}CO emissions. The detection limitation restricted by wavelike baseline reaches beyond the signal of those with relatively weak sources. Of those both ^{12}CO and ^{13}CO were detected in 42. We present the central intensity ratio, $\mathcal{R}$, with an average value of 8.14±4.21, ranging mostly

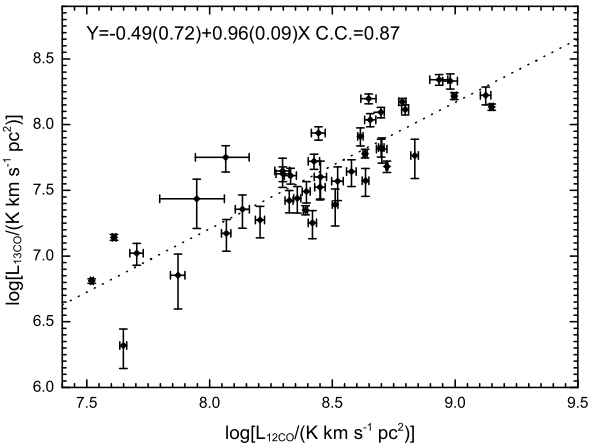

Fig. 2 The comparison between the ^{12}CO and ^{13}CO luminosity. A correlation is validated with C.C. value of 0.87. The dotted line corresponds to the average ratio, $\mathcal{R}$.

from 5 to 13. NGC 4212, NGC 4312, NGC4536, NGC 4631, and NGC 4736 have very low ratios less than 4. This is probably due to systematic uncertainties or a higher optical depth of the gas in the central positions of the galaxies. The uncertainty of $\mathcal{R}$ may not merely indicate the accuracy of our measurement but also reflect pointing errors. The average ratio is slightly lower than previous estimations of 11$\pm$3 (Aalto et al. 1991), 9.3$\pm$3.6 (Sage & Isbell 1991) and 11.3$\pm$3.3 for normal galaxies. Young & Sanders (1986) found no evidence for systematic variation in $\mathcal{R}$ with radius, and Sage & Isbell (1991) did not find clear evidence either. The average of all off-center points is somewhat less than the average of the centers. It is suggested that galaxies which display variations in $\mathcal{R}$ have varying large-scale properties of their molecular cloud distributions. Thus, our lower estimation of the average ratio, $\mathcal{R}$, may not result merely from the different main beam efficiency between telescopes, but also due to the different sample of galaxies with regions larger than the central that are covered in a one beam-size field in our observations.

We compared ^{12}CO luminosity with ^{13}CO luminosity in Fig. 2. Of course a tight correlation can be found because of the same distance and the deviation accounts for variants of $\mathcal{R}$. We could not determine why Taniguchi & Ohyama (1998) claimed that more luminous galaxies have lower ^{13}CO luminosity with respect to ^{12}CO. Perhaps a wider range of CO luminosity data of other galaxies is needed.

Generally, it is suggested that the intensity ratio, $\mathcal{R}$, is a measure of the cloud environment in galaxies Aalto et al. (1991); Aalto et al. (1995). High ratio values ($\mathcal{R} > 20$) might originate in turbulent, high-pressure gas in the centers of luminous interactive galaxies or mergers, intermediate values ($10 \leq \mathcal{R} \leq 15$) refer to normal starbursts, and low values ($\mathcal{R} \simeq 6$) represent the disk population of clouds. The deficiency of ^{13}CO due to isotope-selective photo-dissociation may alternatively account for a high $\mathcal{R}$.

Sage & Isbell (1991) found that the intensity ratio of ^{12}CO/^{13}CO $\mathcal{R}$ is independent of the morphological type. Our result in Fig. 3 is similar to Young et al. (1989) and Sage & Solomon (1989): there is no clear relationship between the intensity ratio, $\mathcal{R}$, and the morphological type evolution in subclasses of spirals.

Fig. 4 illustrates the relationship between $T_{\rm dust}$ and $\mathcal{R}$. It has been claimed that high CO luminosity in luminous far-infrared galaxies are due to a greater excitation temperature of CO gas rather than a higher mass quantity Maloney & Black (1988); Stacey et al. (1991). However, we concluded the same

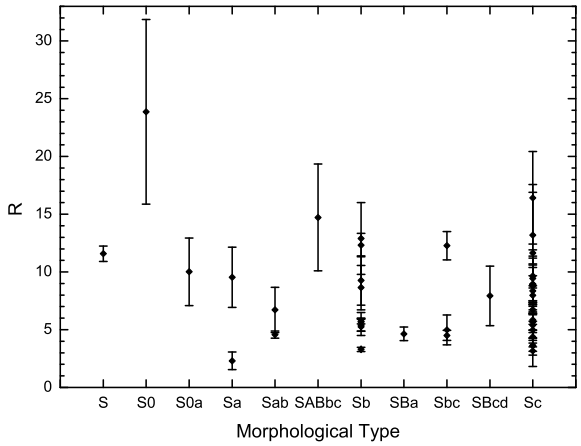

Fig. 3 The intensity ratio of ^{12}CO/^{13}CO, $\mathcal{R}$, is independent of the morphological type. There is no clear relationship between $\mathcal{R}$ and the morphological type evolution in subclasses of spirals.

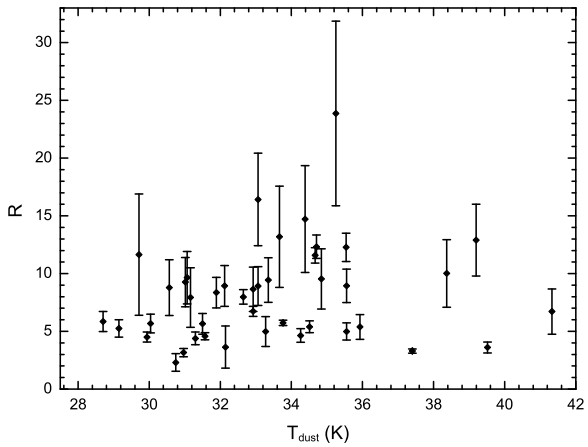

Fig. 4 The correlation between $\mathcal{R}$ and dust temperature. There seems to be little relationship between them below a temperature of 40 K.

results as Sage & Isbell (1991): there seems to be no clear relationship between them below a temperature of 40 K. Unfortunately, we were unable to test whether there exists a trend of $\mathcal{R}$ and $T_{\rm dust}$ beyond 40 K.

The CO-H_2 conversion factor gives us a direct way to estimate H_2 gas in molecular clouds through CO. In the Milky Way, we usually take a universal value of $X = 2 \times 10^{20}$ cm^{-2} (K km s^{-1})$^{-1}$ as an estimation. For an estimation of extragalaxies, we found an average value of $1.44 \pm 0.84 \times 10^{20}$ cm^{-2} (K km s^{-1})$^{-1}$, which is slightly lower than the standard value in the Milky Way.

5 SUMMARY

Using the PMO 13.7-m millimeter-wave telescope, we simultaneously observed the ^{12}CO, ^{13}CO, and C^{18}O J=1−0 rotational transitions in the centers of 58 nearby galaxies with relatively strong ^{12}CO emissions. We detected ^{13}CO emissions in 42 out of the 58 galaxies, but a null detection of C^{18}O emission with a sigma upper limit of 2 mK. The main two results are summarized as follows:

(1) We presented results of spectra, integrated intensity of both ^{12}CO and ^{13}CO emissions in each galaxy. Central beam ratios, $\mathcal{R}$, of ^{12}CO and ^{13}CO range mostly from 5 to 13, with an average value of 8.14±4.21, which is slightly lower than previous estimates for normal galaxies.
(2) We calculated ^{12}CO and ^{13}CO luminosities and clear correlations are validated. We computed the column density of H_2 gas from $I(^{13}\mathrm{CO})$ and then calibrated the X-factor, finding an average value of $1.44 \pm 0.84 \times 10^{20}\ \mathrm{cm}^{-2}\ (\mathrm{K\ km\ s}^{-1})^{-1}$, which is slightly lower than the standard value in the Milky Way.

Acknowledgements Special thanks to the PMO Qinghai Station staff for their help.

References

Aalto, S., Booth, R. S., Black, J. H., & Johansson, L. E. B. 1995, A&A, 300, 369
Aalto, S., Johansson, L. E. B., Booth, R. S., & Black, J. H. 1991, A&A, 249, 323
Braine, J., Combes, F., Casoli, F., et al. 1993, A&AS, 97, 887
Daddi, E., Elbaz, D., Walter, F., et al. 2010, ApJ, 714, L118
Elfhag, T., Booth, R. S., Hoeglund, B., Johansson, L. E. B., & Sandqvist, A. 1996, A&AS, 115, 439
Gao, Y., & Solomon, P. M. 2004, ApJ, 606, 271
Helfer, T. T., Thornley, M. D., Regan, M. W., et al. 2003, ApJS, 145, 259
Leroy, A. K., Walter, F., Bigiel, F., et al. 2009, AJ, 137, 4670
Maloney, P., & Black, J. H. 1988, ApJ, 325, 389
Nishiyama, K., Nakai, N., & Kuno, N. 2001, PASJ, 53, 757
Paglione, T. A. D., Wall, W. F., Young, J. S., et al. 2001, ApJS, 135, 183
Rickard, L. J., Palmer, P., Morris, M., Zuckerman, B., & Turner, B. E. 1975, ApJ, 199, L75
Sage, L. J., & Isbell, D. W. 1991, A&A, 247, 320
Sage, L. J., & Solomon, P. M. 1989, ApJ, 342, L15
Sakamoto, K., Okumura, S. K., Ishizuki, S., & Scoville, N. Z. 1999, ApJS, 124, 403
Sanders, D. B., Mazzarella, J. M., Kim, D.-C., Surace, J. A., & Soifer, B. T. 2003, AJ, 126, 1607
Sanders, D. B., & Mirabel, I. F. 1996, ARA&A, 34, 749
Solomon, P. M., & de Zafra, R. 1975, ApJ, 199, L79
Solomon, P. M., Downes, D., Radford, S. J. E., & Barrett, J. W. 1997, ApJ, 478, 144
Solomon, P. M., & Sage, L. J. 1988, ApJ, 334, 613
Solomon, P. M., & Vanden Bout, P. A. 2005, ARA&A, 43, 677
Stacey, G. J., Geis, N., Genzel, R., et al. 1991, ApJ, 373, 423
Tan, Q.-H., Gao, Y., Zhang, Z.-Y., & Xia, X.-Y. 2011, Research in Astronomy and Astrophysics, 11, 787
Taniguchi, Y., & Ohyama, Y. 1998, ApJ, 507, L121
Wilson, T. L., Rohlfs, K., & Hüttemeister, S. 2009, Tools of Radio Astronomy (Springer-Verlag)
Young, J. S., & Sanders, D. B. 1986, ApJ, 302, 680
Young, J. S., & Scoville, N. Z. 1991, ARA&A, 29, 581
Young, J. S., Xie, S., Kenney, J. D. P., & Rice, W. L. 1989, ApJS, 70, 699
Young, J. S., Xie, S., Tacconi, L., et al. 1995, ApJS, 98, 219